I&EC research
Industrial & Engineering Chemistry Research

pubs.acs.org/IECR

Article

Silica Fume Formation in Different Gas Atmospheres

Vegar Andersen,* Kristian Etienne Einarsrud, Azam Rasouli, and Gabriella Tranell

Cite This: *Ind. Eng. Chem. Res.* 2023, 62, 4246–4259

Read Online

ACCESS | Metrics & More | Article Recommendations | Supporting Information

ABSTRACT: Silica fume is an important byproduct from the silicon production process, with mainly concrete and refractory applications. In this work, the effect of different combustion gas atmospheres on the properties of silica fume has been investigated through small-scale experiments and a pilot-scale experiment. In the small-scale experiments, SiO gas was formed and reacted with four mixtures of nitrogen fixed at 79 vol %, oxygen, carbon dioxide, and carbon monoxide. No significant difference between the particulate matter (PM) formed was found when replacing O_2 with CO_2 using a holding temperature of 1700 °C, when measuring the specific surface area (SSA), particle size distribution, or carbon content. PM formed at a holding temperature of 1650 °C was found to have a significantly higher SSA of 32.9 m^2/g compared to the SSA of 22.3 m^2/g formed at 1700 °C with the same gas mixtures. Condensation products were only found when replacing O_2 with CO, where brown PM was formed through SiO reacting with SiO_2, SiC, and Si. Using a pilot-scale setup, the combustion gas for the silicon process was altered by recirculating different ratios of flue gas back to the furnace hood. Silica fume samples were collected during several tapping cycles with varying flue gas recirculation (FGR) rates. The SSA was measured for the sampled PM and correlated to a selection of operational parameters. A significant negative correlation was found between the SSA of PM and the concentration of H_2O and SO_2 in the off-gas, while a significant positive correlation was found between the SSA and the temperature of the off-gas, the concentration of dust in the off-gas, and the NO_X generation during the process. These results indicate that the temperature and SiO concentration during combustion are more important than the CO_2 (or O_2) concentration in the combustion atmosphere. Using FGR to increase the CO_2 concentration in the off-gas should not change the silica fume particle size, if the H_2O content is controlled.

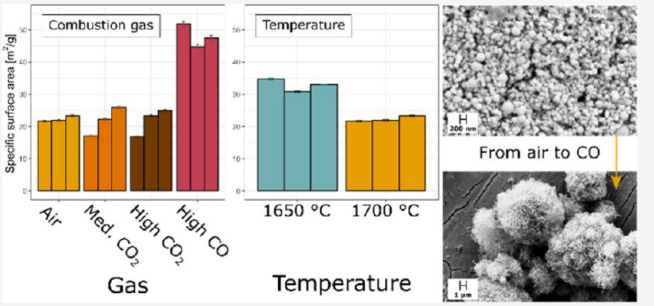

INTRODUCTION

During carbothermal production of metallurgical-grade silicon in submerged arc furnaces (SAF), a significant amount of fine SiO_2 particles, called silica fume, are formed along with silicon in the reduction process. Silica fume is formed in a semiclosed furnace hood, where the process gas meets excessive amounts of air to ensure complete combustion and sufficiently low temperatures for the off-gas system. The silicon yield describes how much silica fume is formed and determines how much carbon the process needs, which is expressed as R1.[1]

$$SiO_2 + (1 + x)C = xSi + (1 - x)SiO + (1 + x)CO \quad (R1)$$

Initially a waste product, silica fume is today used as an important addition to concrete, refractory materials, and a range of other products and hence is considered an important byproduct of the silicon production process.[2] The added fine silica fume, usually with a specific surface area (SSA) around 20 m^2/g, acts as a pozzolan in concrete and adds strength, decreases thermal expansion, and increases corrosion resistance in the concrete product. The purity of the silica fume is important for the end-product application. Elemental silicon is an impurity that should be limited in silica fume due to safety. Silicon can react with pore water in the concrete and slowly evolve hydrogen or hydrogen sulfide, according to R2 or R3. This could lead to dangerous H_2 or H_2S concentrations if it occurs in closed-off concrete installations with limited air circulation. A review of the effects of silica fume in concrete can be found in the guide by the American Concrete Institute.[3]

$$Si_{metal} + 2H_2O = 2H_2 + SiO_2 \quad (R2)$$

$$Si_{metal} + SO_4 + 2H_2O = 2H_2S + 2SiO_2 + OH^- \quad (R3)$$

Carbothermal reduction of silica leads to emissions of CO_2 through combustion of the CO formed in R1. Carbon capture (CC) may be an option for reducing the footprint of silicon production, either by sequestration (CCS) or utilizing the captured CO_2 for purposes that displace the use of other fossil materials (CCU). There are several ways CCU/S can be

Received: November 4, 2022
Revised: February 10, 2023
Accepted: February 13, 2023
Published: March 3, 2023

implemented, and an extensive review of the subject has been done by Gür.[4] A common way of classifying CC is by pre-combustion capture, oxyfuel combustion, or post-combustion capture. Pre-combustion capture, which is the method of capturing CO_2 from the fuel before combustion, is not an option for silicon production as solid carbon is needed for the reduction process of SiO_2 into Si. For CC through oxy-fuel combustion, air is replaced with O_2 under combustion, avoiding diluting N_2 and giving an off-gas with a very high concentration of CO_2. This could be an option for silicon production but requires closing of the furnace. Previous attempts at closing the furnace have been done by Elkem in 1981[5] and by Dow in the 1990s,[6,7] with a motivation of improving the process and producing a sellable combustion gas, consisting mainly of CO and some H_2. These efforts showed a wide range of challenges that needed to be solved to make a closed furnace process viable. One of these challenges was maintaining the product quality of the silica fume. Neither of these efforts made it to a full industrial implementation, and today the open or semiclosed hood is a common configuration for silicon SAFs. Having a closed furnace with oxyfuel combustion and flue gas recirculation (FGR) for temperature control could be a potential solution with a CO_2-rich off-gas and good silica fume quality. This would however require much research and development. The last option is post-combustion capture. With this method, CO_2 is separated from the off-gas after combustion. N_2 in the combustion of air dilutes the CO_2 concentration, and for the silicon process excess air is introduced for the combustion of process gases to control the temperature of the off-gas. The result is an off-gas with a low concentration of CO_2, typically in the range of 1−5 vol % CO_2. Even though the CO_2 concentration in the off-gas from the silicon process is low, post-combustion capture technologies have the advantage of being able to be retrofitted to existing smelters with little to no modification of the smelting process. For this reason, optimization of the silicon process for post-combustion CC has been the motivation of this work. Making CC economically viable for silicon production is a challenge, partly due to the low concentration of CO_2 in the process off-gas.[8] Increasing the concentration of CO_2 in the off-gas would reduce the cost of capturing the CO_2.[9]

Other recent efforts by the current authors to optimize the silicon process have investigated the option of FGR to increase the CO_2 concentration in the furnace off-gas and hence enable potential future CC processes.[9,10] This could be a method of increasing the CO_2 concentration in the furnace off-gas while still having a semiclosed furnace and complete combustion of volatiles and process gases. However, there are still uncertainties about how different combustion gases will change the characteristics of the silica fume formed.

Industrially, the formation of silica fume occurs through R4 as SiO gas escapes the furnace burden and meets air in the furnace hood. Replacing some of the air used for combustion with recirculating flue gas would reduce the oxygen concentration in the combustion gas entering the furnace hood where the silica fume is formed. This could change the properties of the silica fume. Reduced oxygen availability could cause incomplete combustion of volatiles and soot and could also influence the particle formation and growth. Several authors have described the mechanisms of particle formation and growth to produce fumed silica, but there is limited literature available describing in detail how silica fume is formed. Note that silica fume and fumed silica are both fine particulate matter (PM) of SiO_2 but two very different products. Where silica fume is the byproduct of silicon and ferrosilicon production, fumed silica is SiO_2 produced by flame pyrolysis of a vapor phase, often silicon tetrachloride.[11]

Ulrich et al.[12−14] published a fundamental work in the 1970s, showing that the particles formed in combustion processes grow into larger particles through coalescence driven by Brownian collisions, not being limited by reaction or nucleation rates. Pratsinis et al. have published several review articles on the subject of fumed silica[15−17] along with the fundamental principles described by Friedlander.[18] The main drivers for particle growth are temperature, retention time over a critical temperature, and volume concentration of the substance growing into particles. All these studies are however focused on the process of producing fumed silica through flame pyrolysis. Silica fume is formed in very different conditions in the SAF hood, with varying fuel mixtures, as the production and flowrate of process gas change both with time and space within the furnace charge. Estimating particle growth for this process is therefore challenging. González-Fariña[19] established a mathematical model describing silica fume particle formation, emphasizing the importance of the mass flow conditions of the process in particle growth in addition to the chemical reaction, nucleation, and growth through Brownian collisions. Kamfjord investigated silica fume formation from SiO combustion with focus on how SiO combustion can be a source for thermal NO_X generation in the process. He showed that SiO combustion is a major source of heat which causes thermal NO_X generation through the Zeldovich mechanism.[20]

While González-Fariña used reaction R4 as the base reaction for SiO_2 formation, other reactions will occur as the O_2 concentration is reduced. As O_2 is partly replaced with CO_2, some of the formation is expected to shift toward R5 which would reduce the reaction enthalpy[21] and heat available for particle growth. If O_2 is reduced sufficiently for CO to be the most prevalent other gas species, some SiO gas would also start to react according to R6 and R7, forming either SiC or free silicon in addition to SiO_2, which are unwanted from a silica fume product perspective. These reactions are frequently called condensation reactions in metallurgical texts as the products form from the process gas, even though it strictly is not condensation but a gas−gas reaction. Broggi et al. have given an overview of the subject[22] and also characterized the different reaction products.[23] Broggi described that condensates containing elemental silicon appear brown, while SiC-containing condensates often appear blue or white. Quenching SiO gas would produce an amorphous brown condensate consisting of Si and SiO_2, while slower cooling rates would allow the formation of crystalline silicon and cristobalite. Note that these condensation products do not typically grow as spheres as normal silica fume but rather as a layer on a substrate or as wires through an oxide-assisted growth mechanism according to Broggi et al.[24]

$$SiO_{(g)} + 1/2O_{2(g)} = SiO_2 \qquad \Delta G_{1700^\circ C}: -298\ kJ/mol \tag{R4}$$

$$SiO_{(g)} + CO_{2(g)} = SiO_2 + CO_{(g)} \qquad \Delta G_{1700^\circ C}: -186\ kJ/mol \tag{R5}$$

$$SiO_{(g)} + 1/3CO_{(g)} = \frac{2}{3}SiO_2 + \frac{1}{3}SiC \qquad \Delta G_{1700^\circ C}: -33.9\ kJ/mol \tag{R6}$$

https://doi.org/10.1021/acs.iecr.2c03987
Ind. Eng. Chem. Res. 2023, 62, 4246−4259

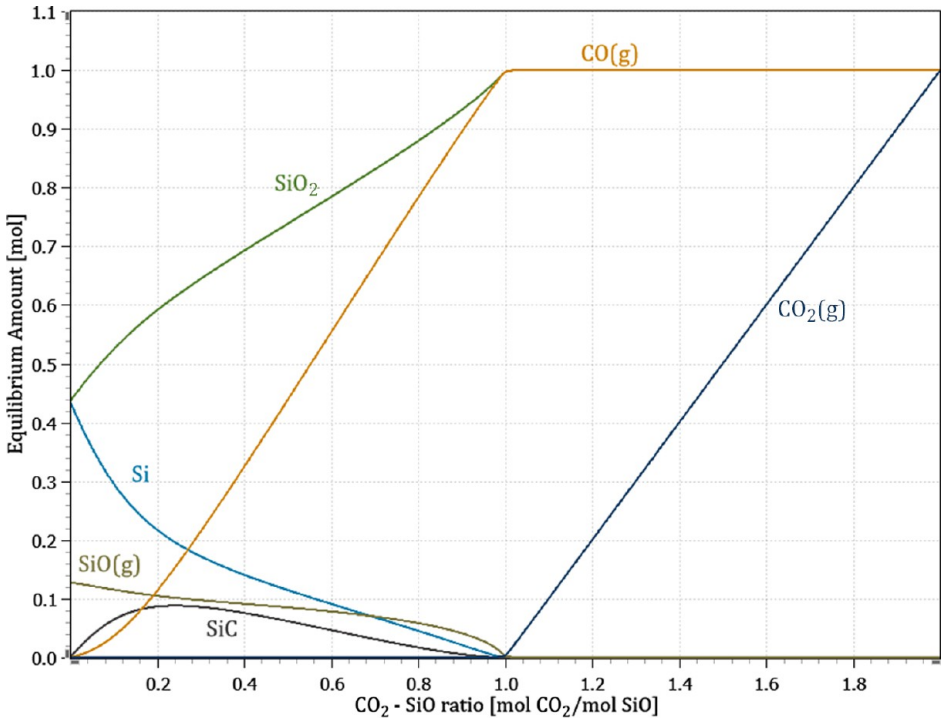

Figure 1. Equilibrium phase composition at 1700 °C for the system starting with 1 mol SiO and CO_2, with increasing CO_2 to SiO molar ratio. At molar ratios under 1 mol CO_2 per mol SiO, all CO_2 is reduced to CO. Calculations are performed using HSC 10.[21]

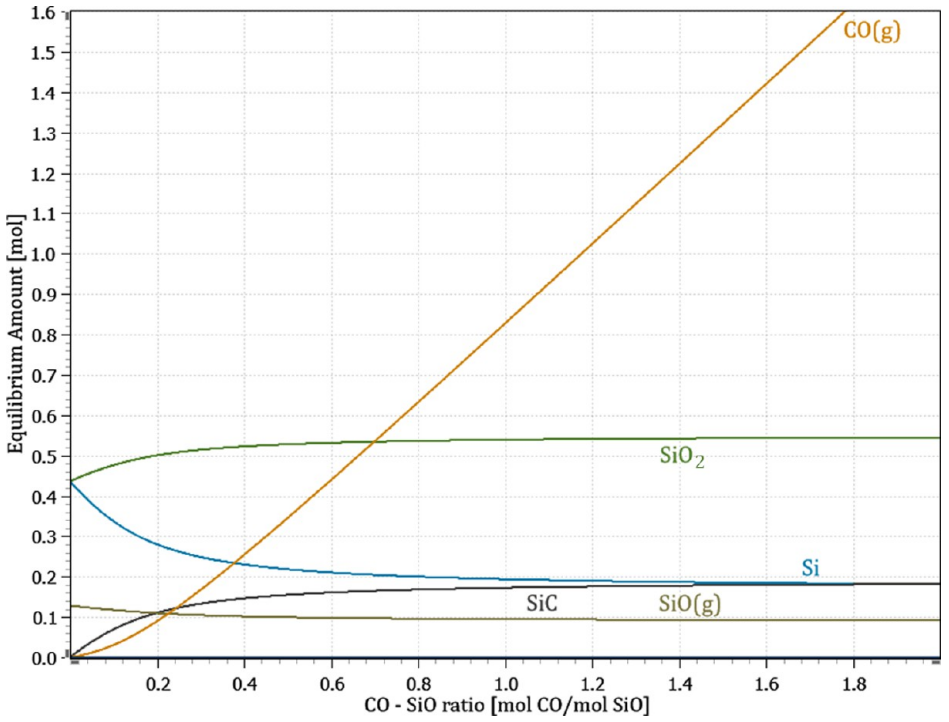

Figure 2. Equilibrium diagram showing stable phases for the system starting with 1 mol SiO and CO, with increasing CO to SiO molar ratio. Calculations were done using HSC 10.[21]

$$SiO_{(g)} = 1/2Si + \frac{1}{2}SiO_2 \qquad \Delta G_{1700^\circ C}: -20.2\ kJ/mol \tag{R7}$$

Considering the equilibrium of different reactions, SiO_2 is the most stable condensed phase at 1700 °C with a surplus of either O_2 or CO_2. The products of R6 and R7, Si and SiC, are stable phases when the molar ratio of CO_2 to SiO gas is less than 1. Figure 1 shows equilibrium compositions at 1700 °C for different CO_2 to SiO molar ratios, calculated using the HSC software[21] and illustrates how the condensation reaction products are more stable with a CO_2 to SiO ratio less than 1. The stable phases for SiO in CO are shown in Figures 2 and 3. Only a small portion of CO reacts to form SiC and almost twice as much Si as SiC is formed at 1700 °C. This changes with

https://doi.org/10.1021/acs.iecr.2c03987
Ind. Eng. Chem. Res. 2023, 62, 4246−4259

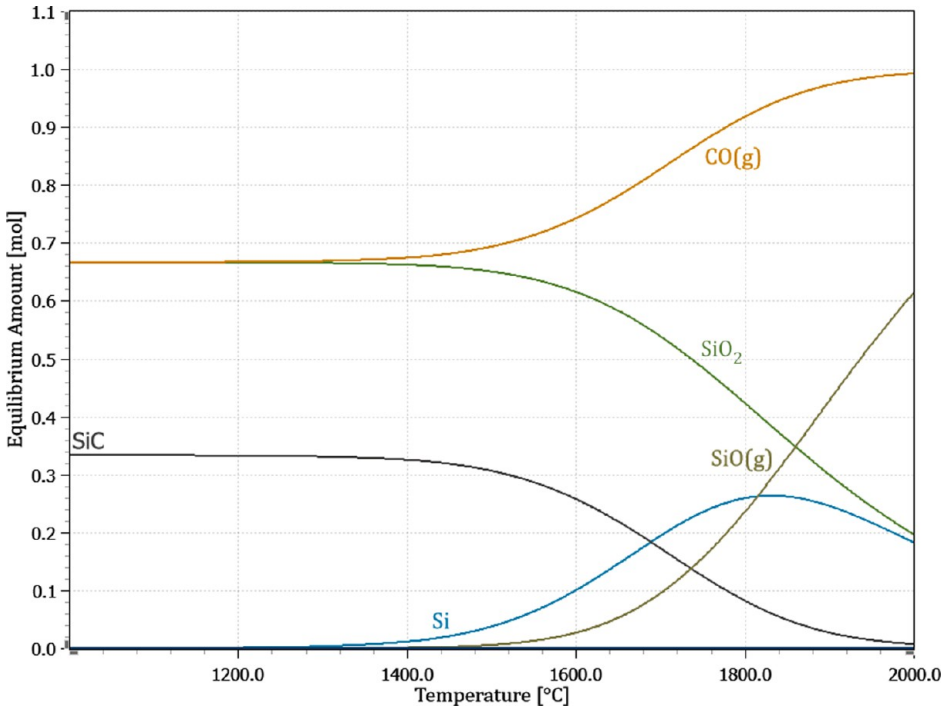

Figure 3. Equilibrium diagram showing the temperature dependence of the stable phases for 1 mol SiO gas mixed with one mol CO gas from 1000 to 2000 °C. Calculations were done using HSC 10.[21]

decreasing temperature, and at temperatures below 1200 °C, only SiC and SiO_2 are thermodynamically stable. The distribution between Si and SiC is most likely kinetically determined based on the cooling rates of the gases.

The aim of this work has been to investigate the effect of combusting SiO gas with gas mixtures of N_2 and different concentrations of O_2, CO_2, and CO to see how this changed the properties of the silica fume and when, and to what extent, the condensation products Si and SiC were formed. This knowledge can be used as a reference to future modeling and would also be helpful to evaluate viable FGR rates for an industrial silicon process.

EXPERIMENTAL SECTION

With this aim in mind, combustion of SiO gas with different combustion gas compositions was conducted in small-scale experiments to isolate the effect of gas compositions. The resulting PM has been investigated by scanning electron microscopy (SEM), and the particle morphology has been mapped out by laser scattering (LS) measurements and SSA measurements with nitrogen adsorption. These measurements were then compared to manual measurements of particle sizes using SEM images of a few samples. LECO analyses were performed to quantify the carbon and oxygen content in the PM from one parallel for each gas mixture. One sample parallel from each gas mixed was investigated using X-ray diffraction (XRD) to identify crystalline phases and quantify amorphous content. For the samples formed in a high CO mix, all parallels were investigated. Silica fume samples from a pilot-scale experiment, where the silicon process was run fully with different FGR rates,[10] were also investigated. SSA for these samples have been measured and correlated to operational conditions during the experiment.

Combustion of SiO gas was tested with different combustion gases in a small-scale setup as illustrated in Figure 4. Gaseous SiO was formed by heating 100 g of a commercial, condensed SiO material to 1700 °C in a closed graphite crucible contained in an Inductotherm 75 kW induction furnace. The SiO material was acquired from Merck Patinal evaporation material (CAS number 10097-28-6). Mixed gas was injected through a lance positioned 5 cm over the bottom of the crucible, and the reacted gas and PM flowed out through a cooled tube into a filter box where the PM was collected. Four different gas mixtures were tested with the same flowrate of 5 L per minute. Table 1 shows the different gas mixtures used in the setup. All gases used were instrument grade and delivered by Linde Gas.

The temperature was measured using a C-type thermocouple which was connected to a Eurotherm 3508 temperature controller that regulated the power of the induction furnace to achieve the desired ramp-up and holding temperatures. Gas injection was started when the holding temperature of 1700 °C was reached and continued for 45 min before shutting down. One series of three parallels was also run with a holding temperature of 1650 °C using synthetic air as the combustion gas to investigate how sensitive the setup was for different temperatures. A decreased holding temperature would decrease the equilibrium partial pressure of SiO in the crucible and limit the amount of external energy for particle growth and produce silica fume with a higher SSA. The external energy supplied through the heating of graphite was only necessary for creating the precursor SiO gas and not necessary for the particle growth itself. Since gas injection and SiO combustion occurs in the same place where the SiO gas is formed, it was not possible to decouple SiO partial pressure and the extra energy added through the graphite crucible.

Gas and particles exiting the crucible were cooled in a water-cooled tube before entering the filter box. Inside the filter box, a glass fiber filter, coated with a polytetrafluoroethylene membrane, separated the PM from the gas. After each experiment, the PM was collected for analysis and a new filter

https://doi.org/10.1021/acs.iecr.2c03987
Ind. Eng. Chem. Res. 2023, 62, 4246−4259

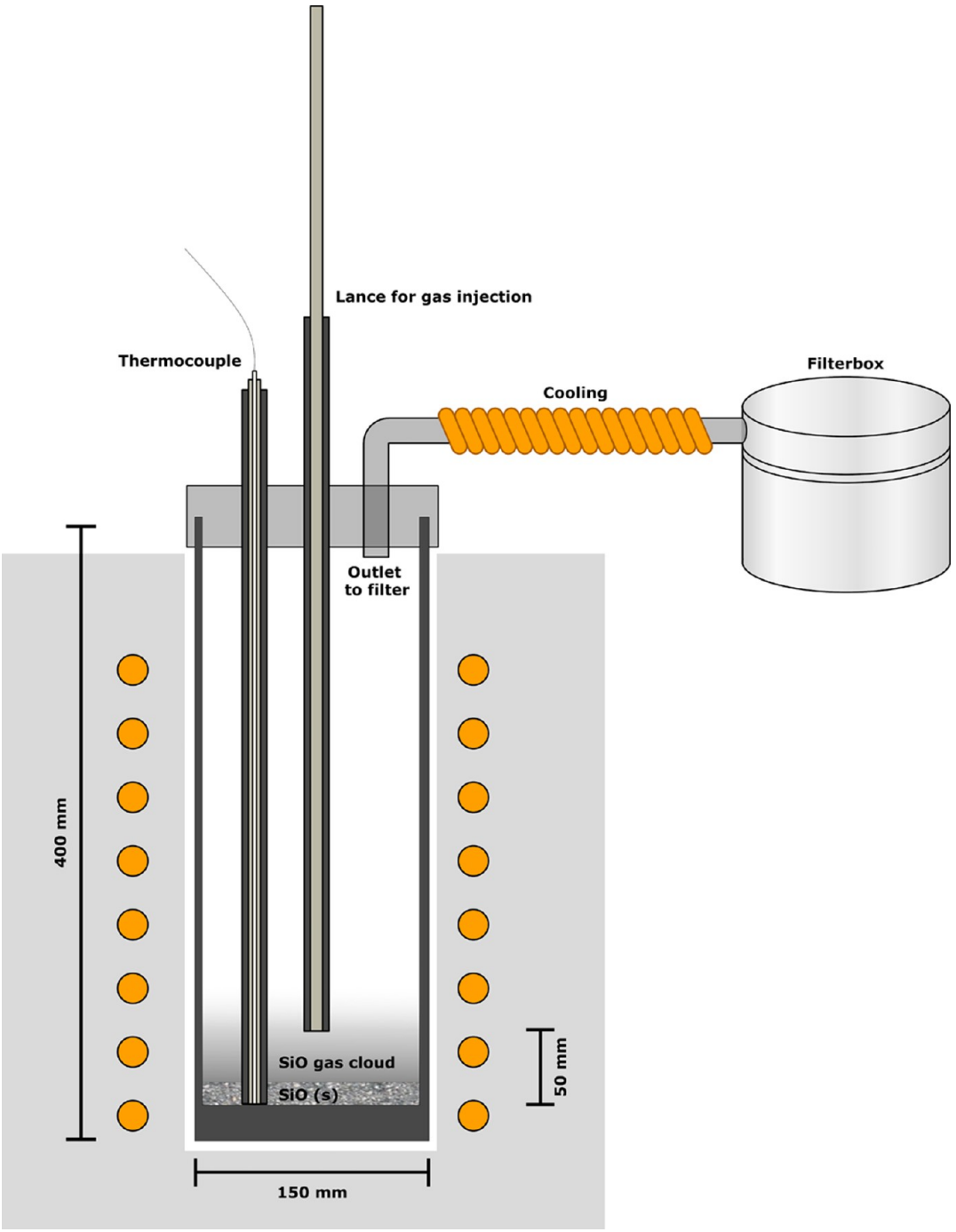

Figure 4. Illustration of the small-scale crucible and filter setup.

Table 1. Gas Mixtures Tested in the Small-Scale Setup[a]

	N_2 [vol %]	O_2 [vol %]	CO_2 [vol %]	CO [vol %]
synthetic air	79	21	0	0
medium CO_2	79	9	12	0
high CO_2	79	0	21	0
high CO	79	0	0	21

[a]Three experimental runs were performed with each gas mixture giving three parallel PM samples.

placed inside the filter box. For each gas mix, three experiments were conducted, giving three parallels and three samples of PM for each mix.

The pilot-scale experiment was a full production process experiment with industrial raw materials to test the concept of FGR, described in detail by Andersen et al.[10] Figure 5 illustrates the setup used and the location for particulate sample collection and gas analysis. Increasing rates of FGR gave an increase in CO_2, H_2O, and other flue gas species at the expense of oxygen concentration as air was replaced by filtered flue gas. Particles were extracted from the off-gas stream iso-kinetically, using a gas probe and nozzle connected to a filter for particle extraction and a vacuum pump for gas extraction, shown in Figure 6. Using the ITES software from Paul Goethe GmbH, the flowrate of the sampling line was adjusted to match the flowrate inside the off-gas pipe.

https://doi.org/10.1021/acs.iecr.2c03987
Ind. Eng. Chem. Res. 2023, 62, 4246−4259

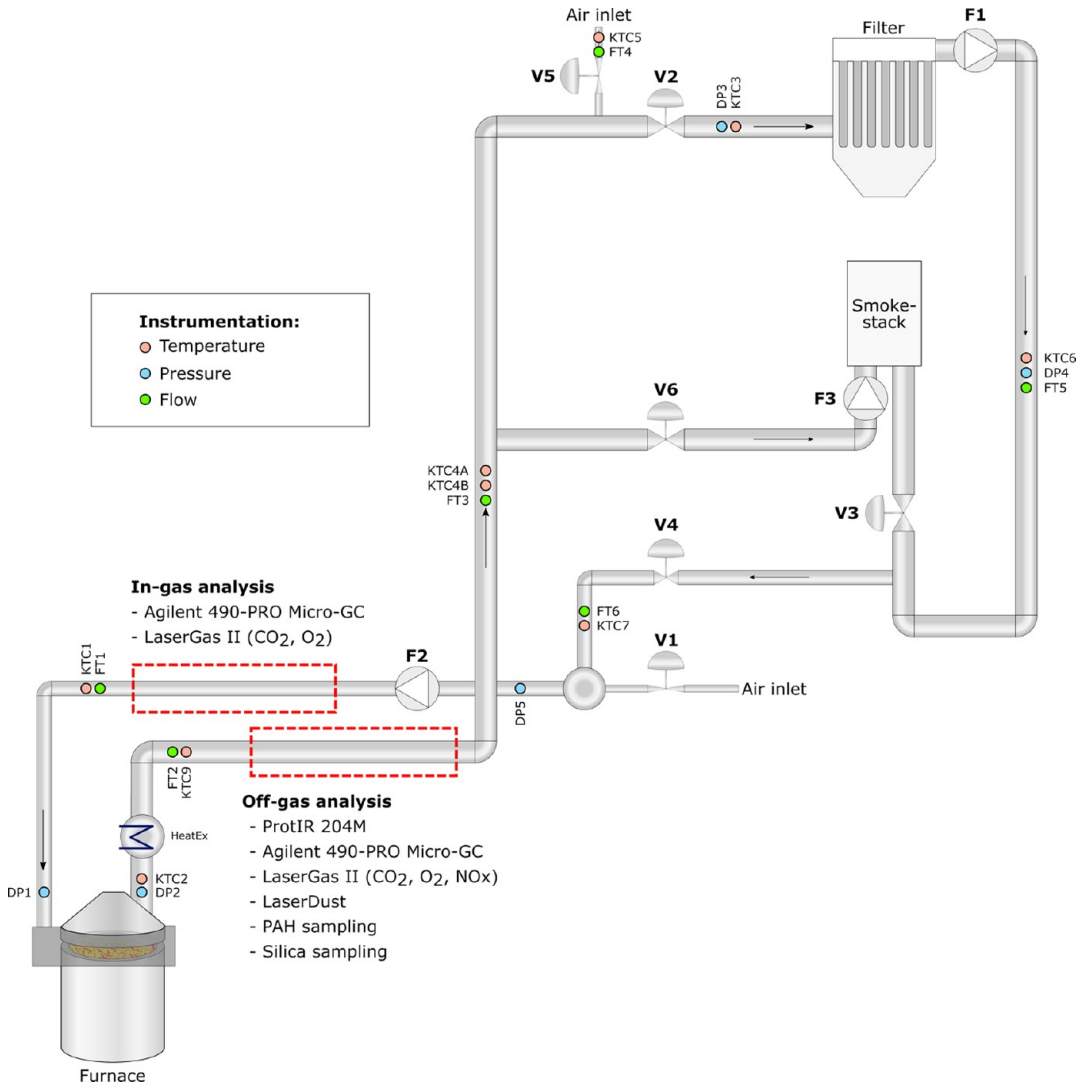

Figure 5. Illustration of the pilot-scale setup for testing the FGR, reprinted from ref 25. Copyright 2022 The Minerals, Metals & Materials Society. Used with permission.

PM Analysis. SSA was measured for all PM samples both from the small-scale experiments and the pilot-scale experiment. The measurements were performed with a 3Flex 3500 instrument from Micromeritics using a 5-point BET method. Degassing of all samples was done using a Degas SmartPrep instrument with a holding time of 5 h at 300 °C with nitrogen purging.

SEM imaging of a selection of samples was performed using a Zeiss SUPRA 55-VP scanning electron microscope. The samples were dispersed in acetone and held in an ultrasound bath for 1 min before a few drops were transferred to a sample holder using a pipette. The sample holders with the samples were then dried at 60 °C, before a thin gold coating was applied for good electrical conduction. A primary particle-size distribution (PSD) was generated using the SEM pictures of each sample and measuring a random selection of particles using the software ImageJ.

LS measurements to obtain PSDs were carried out using a HORIBA Partica LA-960. These measurements were only performed on the small-scale experiment samples. Water was used as the fluid, and the refractive index was set to 1.53[26] for the silica fume and 1.333 for water. All samples were measured before and after applying 10 min of ultrasound treatment to see if ultrasound would break up any agglomerates or aggregates. The PSD found by LS was compared to the results of the manual particle measurements to determine if LS and ultrasound treatment could be used to measure the primary particle size.

Quantification of carbon and oxygen was done for one sample for each of the gas mixtures tested. Carbon was quantified using a LECO 844 Series Combustion Analyzer,[27] while oxygen was quantified using a LECO 836 Series Elemental Analyzer.[28] Carbon in the samples was oxidized in oxygen at high temperatures, and the resulting CO_2 was analyzed by non-dispersive infrared (NDIR) cells. Oxygen is measured in a similar way, but oxygen was reacted with a carbon crucible at a high temperature and swept away with an inert carrier gas, and the resulting CO_2 was measured by NDIR cells. All samples were analyzed with XRD. The XRD analysis was performed using a Bruker D8 A25 DaVinci X-ray diffractometer with a Cu (1.54 Å) source and LynxEye SuperSpeed 1D detector, and analysis of the results was done with the Bruker EVA and TOPAS software. The scans were done in the 2θ range of 5−100° using a step size of 0.016° and a time per step of 2 s/step. Quantification of amorphous content was done according to the internal standard

https://doi.org/10.1021/acs.iecr.2c03987
Ind. Eng. Chem. Res. 2023, 62, 4246−4259

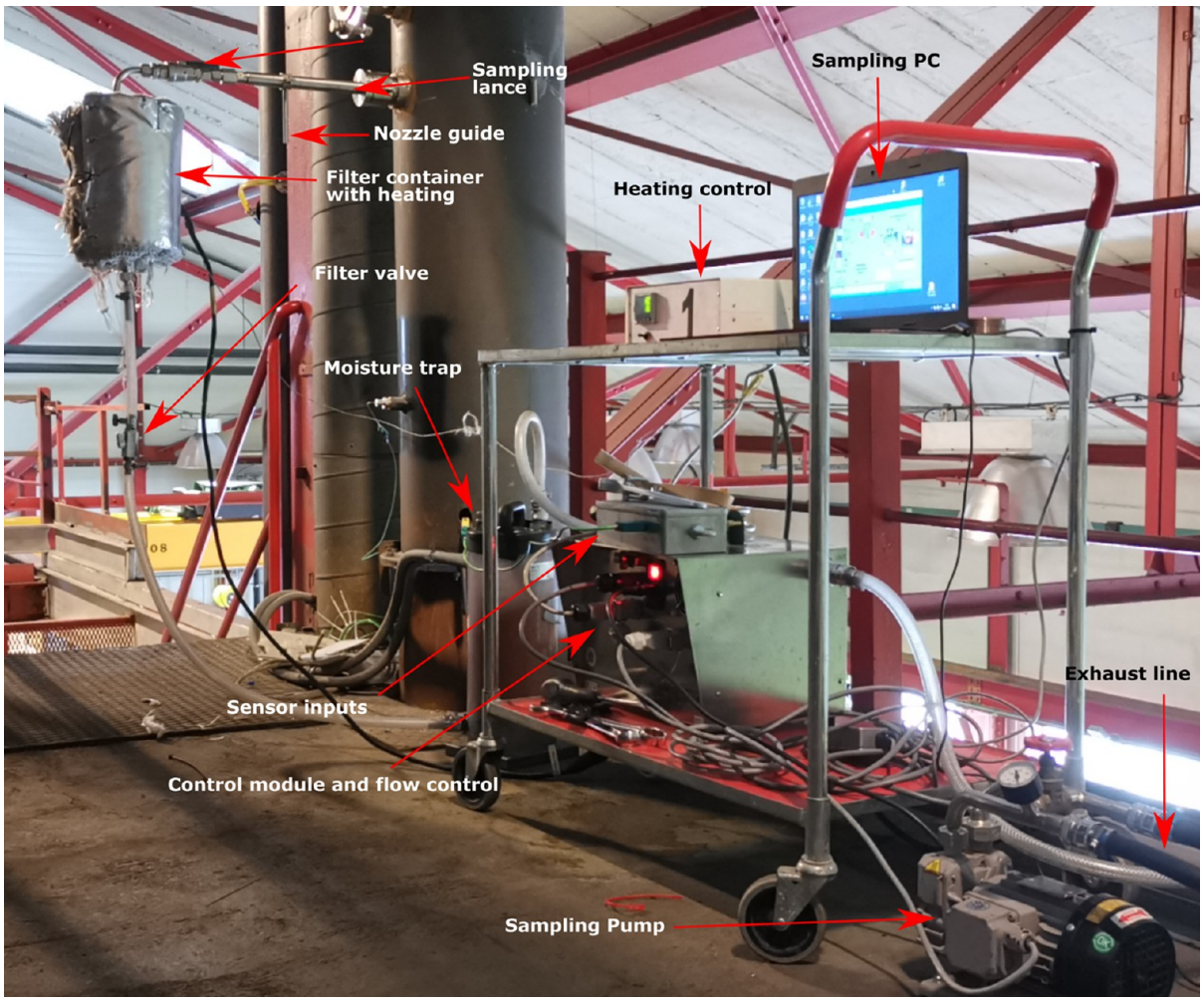

Figure 6. Sampling setup used for extracting silica fume samples during the pilot-scale experiment.

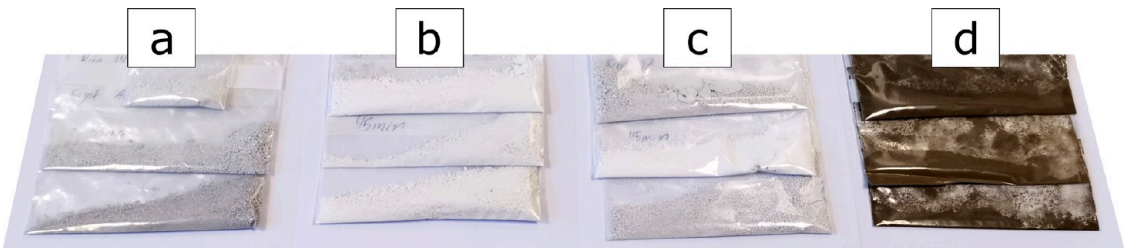

Figure 7. Silica fume samples from small-scale experiments with (a) synthetic air, (b) N_2 + 12% CO_2, (c) N_2 + 21% CO_2, and (d) N_2 + 21% CO.

method, described by Madsen,[29] where the samples were spiked with around 25 wt % alumina. Three parallel samples were analyzed for the quantification of the amorphous content for which the average value has been reported.

RESULTS AND DISCUSSION

Small-Scale Experiments. Samples from the small-scale experiments are shown in Figure 7 and show that products from the experiments with synthetic air or N_2 and CO_2 are similar with small variations in color, although the color varies more between each parallel than between gas mixtures. These samples were white with different shades of light gray and appeared to consist of mainly pure silica fume. Samples from the runs using CO and N_2 gases were markedly different with a dark brown appearance, indicating that the PM had formed from a condensation reaction and not through either of reactions R4 or R5.

Figure 8 shows the result of SSA measurements for all samples made in the small-scale experiment. SSA measurements for the samples formed in synthetic air at 1700 °C show an average SSA of 22.3 m^2/g. For the runs using 12 and 21% CO_2, a slightly lower average SSA was found, with 21.8 and 21.7 m^2/g, respectively, but with more variance between parallels. PM formed in synthetic air at 1650 °C had a SSA of 32.9 m^2/g, while samples produced during the runs with CO gas had a significantly higher SSA, averaging 48 m^2/g. Estimating the particle size from the SSA, using a density of 2.2 g/cm^3 and assuming solid spherical particles with no aggregates, gives an average particle diameter of 122.3 nm for the samples made in synthetic air. Similarly, the corresponding average particle

https://doi.org/10.1021/acs.iecr.2c03987
Ind. Eng. Chem. Res. 2023, 62, 4246−4259

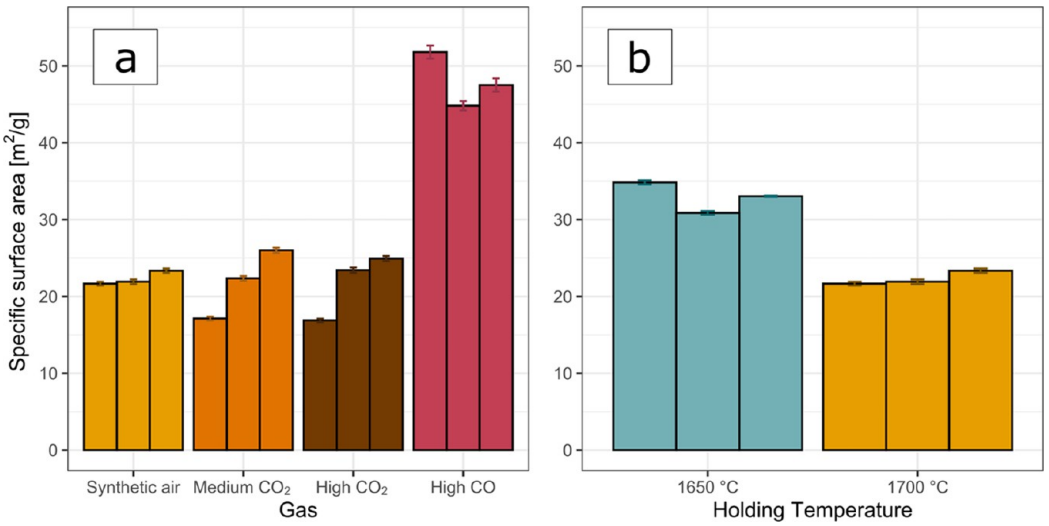

Figure 8. SSA of silica fume samples from the small-scale experiments. (a) shows the SSA for PM formed in different gas mixtures at 1700 °C, while (b) shows the SSA for PM formed at holding temperatures of 1650 and 1700 °C using synthetic air. Each bar represents a parallel experiment, and the error bars give the uncertainty of each measurement.

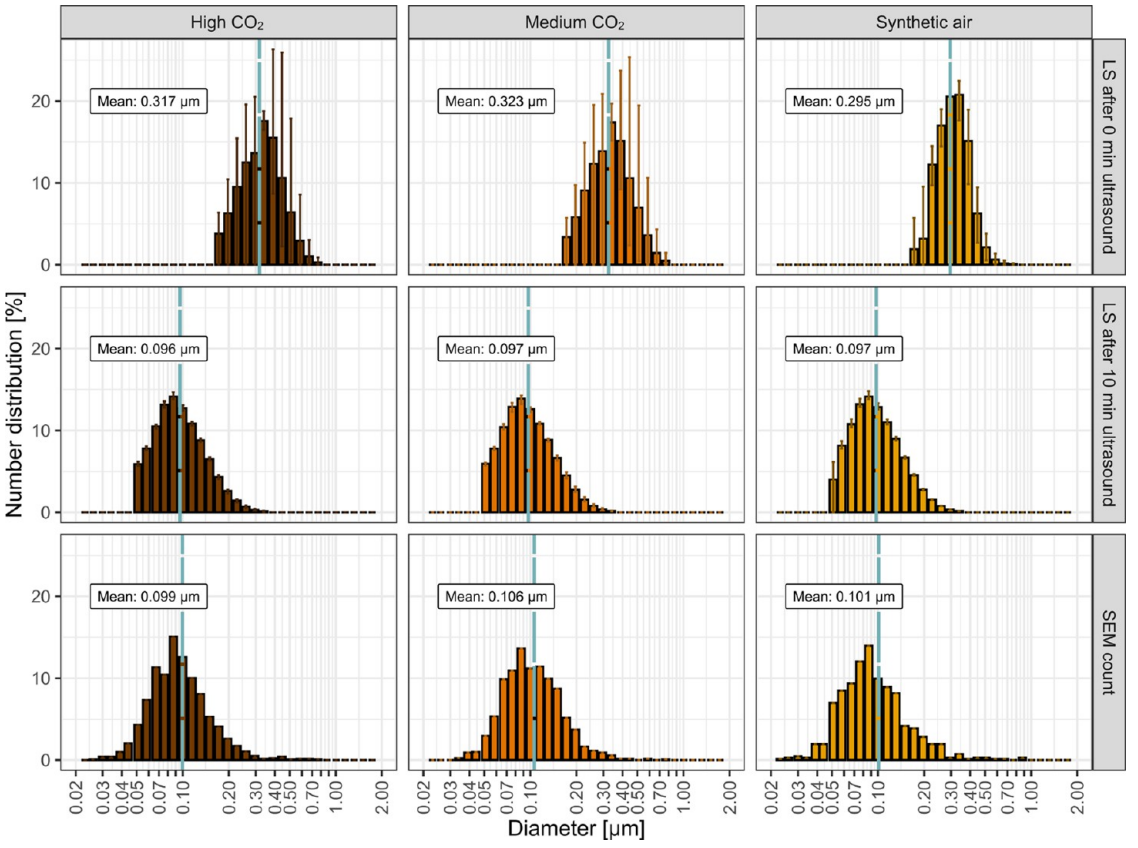

Figure 9. PSDs measured by LS and particle count using SEM images. Roughly 1200 particles were manually measured for the samples made in high- and medium-CO_2 gas each and just under 700 particles for the sample were made in synthetic air. Dashed lines mark the number-average particle diameter.

diameter for samples made in medium and high CO_2 were 125.2 nm and 125.7 nm, respectively, while PM formed at 1650 °C was calculated to have an average particle diameter of 83.1 nm. The PM formed in the high CO runs was found to have a different shape than spheres, and the assumptions for calculating particle size from the SSA were not valid.

LS measurements, shown in Figure 9, corroborated the trend with no significant change in particle size with increasing CO_2 concentration. Both before and after 10 min of ultrasound treatment, the median particle size was similar between the different gases. Increasing ultrasound treatment however shifted the PSD toward smaller particle sizes as agglomerates were dispersed and aggregates were broken down. The PSD based on manually measuring primary particles in the SEM images is also shown in Figure 9 and indicates that the particle size measured by LS, after 10 min ultrasound treatment, was fairly close to the

https://doi.org/10.1021/acs.iecr.2c03987
Ind. Eng. Chem. Res. 2023, 62, 4246−4259

manually measured primary PSD but is missing some of the larger particles. Note that the number of particles measured by LS is significantly higher than the number of particles counted from the SEM images. Counting particles in SEM pictures can also be influenced by selective bias by the human counter. Table 2 summarizes the average particle diameters and standard deviations found using the different measurement methods.

Table 2. Measured and Estimated Average Particle Sizes Based on Number Frequency and Standard Deviation[a]

particle diameter [μm]	high CO_2	medium CO_2	synthetic air
LS after 0 min ultrasound	0.317 ± 0.010	0.323 ± 0.011	0.295 ± 0.007
LS after 10 min ultrasound	0.096 ± 0.004	0.097 ± 0.004	0.097 ± 0.004
SEM count	0.099 ± 0.006	0.106 ± 0.006	0.101 ± 0.007
estimated from SSA	0.122	0.125	0.126

[a]Since the SSA measurements does not give a distribution, only the estimated diameter is given.

Carbon and oxygen contents of the samples measured by LECO are shown in Figure 10. The PM formed using CO gas contains significantly more carbon than the PM that appeared as normal silica fume.

The source of the carbon detected by LECO analysis could come from soot from the reverse Boudouard reaction, R8, as the gas temperature drops toward the filter box. For the PM formed in high CO experiments, another possible source of carbon could be the consumption of SiO through R6 which would form SiC. Oxygen is expected to be found as SiO_2 in the samples. If all PM was SiO_2, then it would contain 53.3% oxygen. This is close to what is found in the samples formed in synthetic air and medium and high CO_2 atmospheres. The oxygen content in PM formed in CO is however significantly lower at 37.5%, which indicates that these samples contain only 70% SiO_2 if all oxygen is bound in SiO_2.

$$C + CO_2 = 2CO \quad \text{(R8)}$$

SEM investigations of the samples confirmed that the particles formed using O_2 and CO_2 in combination with nitrogen were spherical, very similar to the general description of silica fume given by Friede.[30] These are shown in Figures 13−15. The

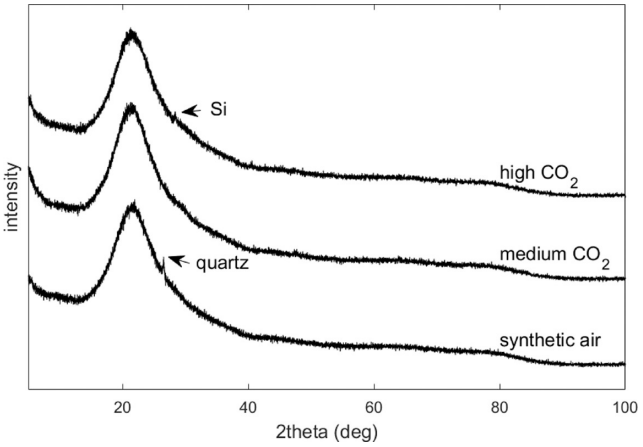

Figure 11. XRD pattern for the samples formed in synthetic air and medium CO_2 and high CO_2 atmospheres.

particles formed using CO and N_2 gas were markedly different. Instead of spheres, typical to amorphous silica fume, the particles appeared to be clusters of wires, shown in Figure 16. Looking at the brown appearance of this PM, it appeared similar to what has been described as a brown condensate by Broggi and Tangstad,[22] Ksiazek,[31] and Vangskåsen[32] and identified as the product of R7 with Si and SiO_2. However, the structure Aarnæs et al.[33] found when investigating SiC formed from SiO and methane gas was similar to what was observed in the samples formed in high CO at higher magnifications. Both Aarnæs and Broggi argued that the wires formed during the condensation of SiO_2 and SiC were formed through an oxide-assisted growth mechanism, where a central SiC wire grows in one direction surrounded by SiO_2. It is plausible that both reactions R6 and R7 are capable of forming one-directional wires through oxide-assisted growth.

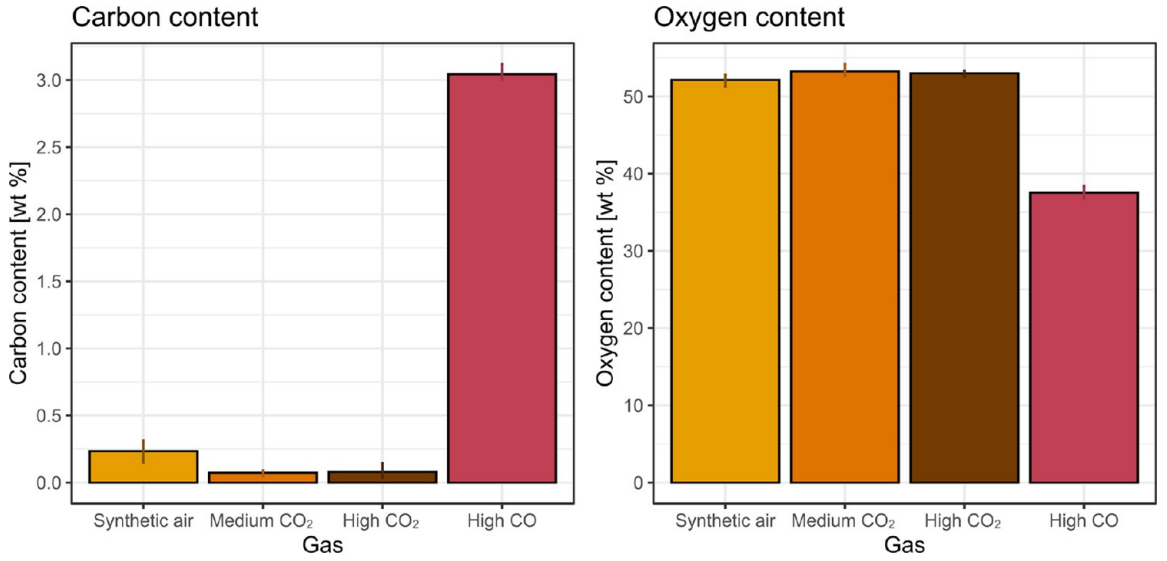

Figure 10. Carbon and oxygen contents in PM for one parallel for each gas mixture from the small-scale experiments. Error bars indicate the maximum and minimum measured for the same sample.

https://doi.org/10.1021/acs.iecr.2c03987
Ind. Eng. Chem. Res. 2023, 62, 4246−4259

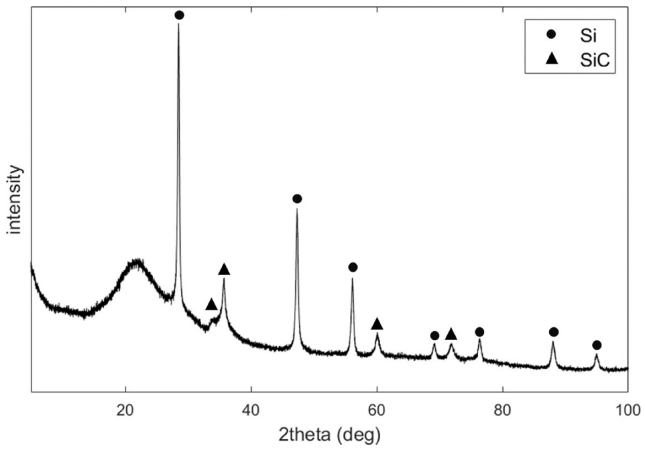

Figure 12. XRD pattern for the PM formed in the high CO atmosphere with silicon and silicon carbide peaks marked.

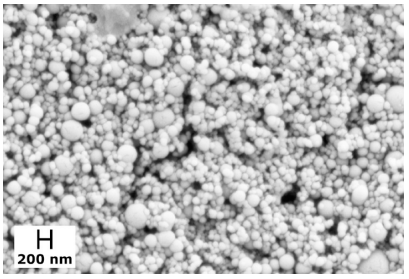

Figure 13. SEM image at 50k magnification of particles formed in a gas of 79% N_2 and 21% O_2 with an SSA of 21.7 m^2/g.

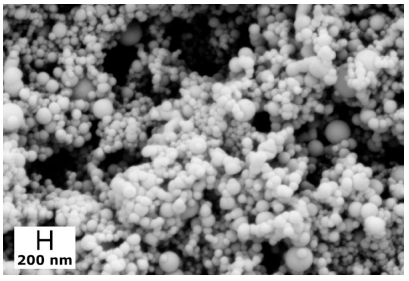

Figure 14. SEM image at 50k magnification of particles formed in a gas of 79% N_2, 9% O_2, and 12% CO_2 with an SSA of 22.4 m^2/g.

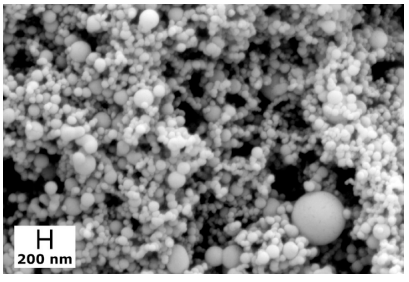

Figure 15. SEM image at 50k magnification of particles formed in a gas of 79% N_2, 0% O_2, and 21% CO_2 with an SSA of 23.4 m^2/g.

XRD analysis of the samples formed in synthetic air and medium and high CO_2 showed an almost exclusively amorphous content, with the exception of traces of crystalline quartz in the synthetic air sample and crystalline silicon in the high CO_2 sample (Figure 11)

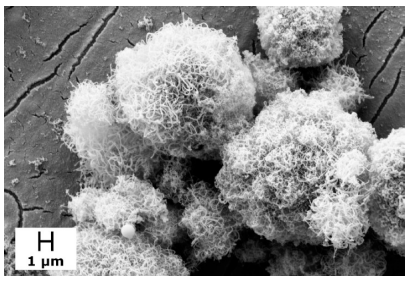

Figure 16. SEM image at 10k magnification of particles formed in a gas of 79% N_2 and 21% CO with an SSA of 44.8 m^2/g.

XRD analysis of the PM formed in high CO detected two crystalline phases, in addition to a significant amount of amorphous content. 83.2 wt % of the sample was found to be amorphous, 10.9 wt % crystalline silicon, and 6.2% crystalline silicon carbide. Figure 12 shows the X-ray diffraction pattern for the analysis, showing the signal found from the silicon phase (PDF 00-027-1402) and the silicon carbide phase (PDF 04-007-1956).

An approximation to the phase composition can be made by combining the XRD quantification and the LECO results. It was assumed that the 37.5 wt % oxygen, measured by LECO, was all bound in 70.5 wt % amorphous SiO_2. Of the 3 wt % C, measured by LECO, 1.9 wt % was bound in the 2.1 wt % SiC, while the remaining 1.1 wt % was amorphous C soot. Summing this up, 70.5 wt % amorphous SiO_2, 10.9 wt % Si, 6.2% SiC, and 1.1 wt % amorphous C adds up to a total of 88.7 wt % total content and 71.6 wt % amorphous content, both with a roughly 11 wt % deficit to their expected values. Since the system was limited to Si, C, O, and the reported potential of brown condensate containing a significant amount of amorphous silicon, it was assumed that the remaining 11 wt % deficit was amorphous silicon. This gave a phase composition of 70.5 wt % SiO_2, 21.9 wt % Si, 6.2 wt % SiC, and 1.1 wt % C soot. With this distribution, 46.9 wt. % SiO_2 would be bound in the $Si-SiO_2$ condensate, 18.6 wt % SiO_2 bound in the $SiC-2SiO_2$ condensate, and the remaining 9.3 wt % as free SiO_2. From the SEM images, some spherical particles were seen in the PM form in high CO gas, but the amount has not been quantified. Thermodynamically R6 has a lower Gibbs energy than R7 throughout the temperature range from 1700 °C and down to room temperature, but the brown condensate formed from R7 is still found in several studies. Despite being thermodynamically less favored than R6, Schei et al.[1] argued that R7 is the most important condensation reaction based on the reaction rate and that it releases less heat with −306 kJ/mol SiO at 1700 °C than R7 with −464 kJ/mol SiO at the same temperature. The phase distribution, estimated above, indicated that the cooling rate in this experimental setup was high enough to favor R7 over R6.

Only spherical particles were seen in the samples from the experiments using only CO_2 and N_2 gases, indicating that no condensation occurred. Although there was no oxygen available in these experiments, a very white PM was formed with the typical silica spheres seen in normal silica fume. The lack of any significant signs of carbon or silicon carbon indicates that the PM in these experiments has formed through R5, where SiO reacts with CO_2 to form the typical silica spheres. Interestingly, the particles formed do not seem to differ much from the particles formed with oxygen present through R4, indicating that CO_2 is a sufficient oxidizer to form normal silica fume particles. It is also interesting to note that SiO gas appears to easily reduce

https://doi.org/10.1021/acs.iecr.2c03987
Ind. Eng. Chem. Res. 2023, 62, 4246−4259

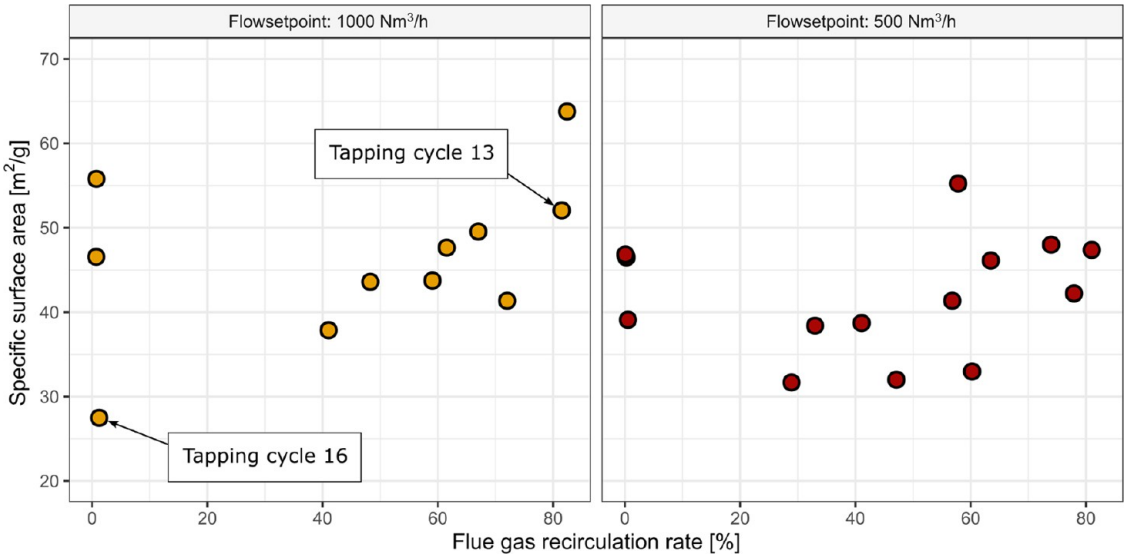

Figure 17. SSA for samples collected at varying FGR rates for the two flowrates used during the pilot experiment. SEM images of PM collected during tapping cycle 13 and 16 can be found in Figures 18 and 19.

CO_2 into CO gas—an interesting aspect in terms of the potential for chemical conversion of CO_2 into CO-rich fuel.

FGR Experiment. For the samples collected during the FGR pilot-scale experiment, all samples appeared to be normal silica fume, with no indication of products from R6 or R7. A varying degree of carbon contamination was apparent from the varying discoloration of the PM. The layer deposited first in the filter often had a darker color, indicating that the sample collection was started before carbon fines and tar had burned off after charging. Concentration of CO_2 was successfully increased using FGR, and the detailed results from this experiment can be found in the previous publications,[25] and a table of average values for each tapping cycle can be found in the Supporting Information.

A wider range of SSA values, from the lowest at 27 m^2/g to the highest at 64 m^2/g, was found when measuring the samples collected from the FGR pilot experiment. Figure 17 shows the SSA for samples collected at different FGR- and flowrates. Each sample was collected over the middle part of a tapping cycle. Sampling was only started when the desired FGR rate was achieved and stopped before the tapping cycle ended mostly because of too high off-gas temperatures to maintain the FGR rate. For some runs, the filters clogged early and ended sampling. Figure 18 shows a SEM image of silica fume from a tapping cycle with a high FGR rate and a high SSA, while Figure 19 shows silica fume with slow SSA formed during a tapping cycle with no FGR.

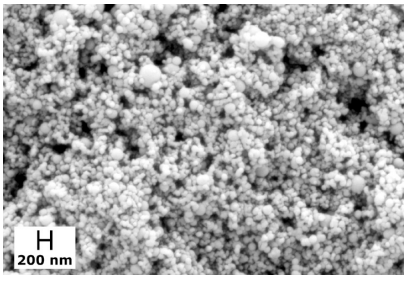

Figure 18. SEM image of PM from tapping cycle 13 of the pilot-scale experiment with the maximum FGR rate at a magnification of 50k. SSA: 52.05.

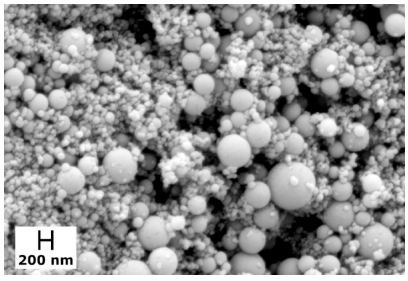

Figure 19. SEM image of PM from tapping cycle 16 of the pilot-scale experiment with no FGR at a magnification of 50k. SSA: 27.48.

It must be emphasized that there were more variations than just the FGR rate between each sampling point. Especially, the rate of SiO combustion, determined by the silicon yield in R1, varied substantially between each tapping cycle.[25] The relation between SSA and dust concentration in the off-gas was the strongest correlation found in the analysis and explains some of the trends seen in Figure 17. Tapping cycles with a high SiO combustion rate and a high dust concentration in the off-gas generally had a low SSA in the sampled PM. Another uncertainty that affected the resulting SSA of the sampled fume was the amount of carbon contamination, where carbon would have a different SSA than the silica fume. Explaining the SSA of the silica fume based on the FGR rate was therefore challenging, but a correlation analysis was attempted to illustrate the main findings.

Figure 20 shows a correlation chart for selected parameters for the pilot-scale experiment. Using a confidence interval of 95% and the Pearson correlation, the analysis shows that the SSA of the silica fume was positively correlated to the FGR rate but not with statistical significance. Note that a correlation between FGR and SSA would be significant if the tapping cycles with no FGR were excluded from the analysis. A significant positive correlation for FGR rate with water content and SO_2 content in the off-gas was found, and a significant negative correlation between the SSA and the temperature of the off-gas, PM concentration, and NO_x concentration in the off-gas, both with

https://doi.org/10.1021/acs.iecr.2c03987
Ind. Eng. Chem. Res. 2023, 62, 4246−4259

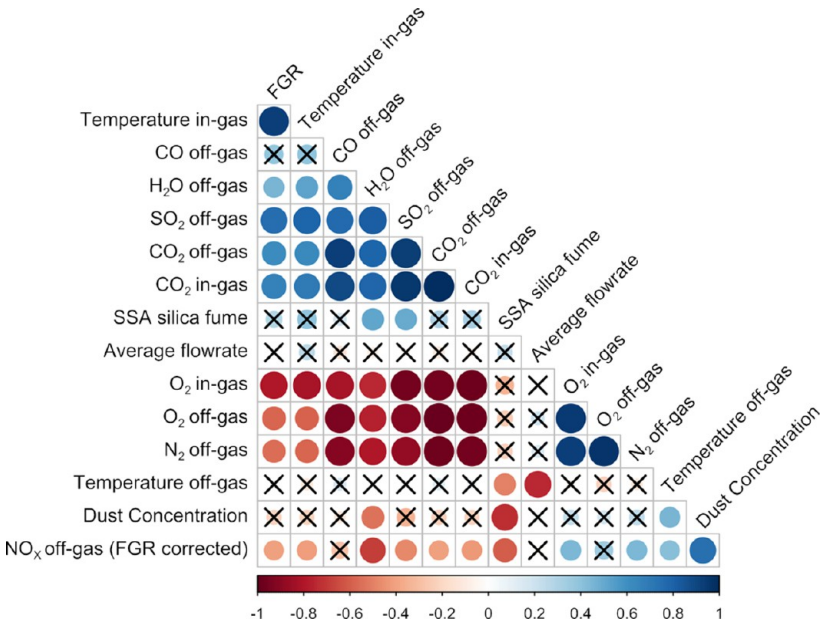

Figure 20. Correlation chart for selected parameters for the pilot-scale experiment. Crossed out circles indicate that the correlation was not significant within a 95% confidence interval.

and without corrections for NO_x recirculated through FGR, was also shown.

Kamfjord et al.[34] found that the time for particle growth and formation time for thermal NO formation was in the same order of magnitude, and it is hence not surprising that a correlation is found between NO_x and particle size in this study. Similarly, the dust concentration was given by the amount of SiO available for combustion, which was the source for the energy needed to form thermal NO and would also facilitate particle growth and reduce SSA.

As for the significant positive correlation between the H_2O and SO_2 content in the off-gas, these are both species expected to increase with increasing FGR as more off-gas is recirculated, in the same way as CO_2 concentration increases with increasing FGR. Although a positive correlation coefficient was found between the SSA and the CO_2 concentration in the off-gas and in-gas, as well as with the FGR rate, this was not within the 95% confidence interval. This is in line with the results of the small-scale experiments, where no real difference between silica fume formed in CO_2 or in O_2 was found. A higher moisture content in the combustion air would limit the adiabatic flame temperature, limit particle growth, and result in a higher SSA. The SO_2 content was governed by the same mechanisms as that for H_2O and has no likely causality to particle formation but may have had a surface-active influence. However, H_2O and SO_2 are species that are vaporized early after charging, and the high SSA in the runs with high H_2O and SO_2 concentrations could have been caused by early start of sampling, coinciding with when the dust generation was low. A low concentration of SiO would give slower particle growth and lower temperatures in the furnace hood. A conclusion to this would need further research.

Industrial Relevance. From the small-scale experiments, it seems that CO_2 oxidized SiO sufficiently well to form good-quality silica fume. No signs of condensation products were seen in these samples, only in the samples formed in the CO atmosphere. This could mean that increasing CO_2 content in the combustion air in an industrial furnace through FGR would not affect the silica fume morphology significantly. No significant correlation was found between CO_2 concentration in the combustion air and the SSA of the silica fume formed in the pilot-scale experiments. However, a significant correlation between the FGR rate and the SSA was found by excluding tapping cycles with no FGR. The correlation between SSA of the PM and CO_2 in the in-gas or off-gas was still not statistically significant after removing these tapping cycles from the analysis. Significant positive correlations were found for H_2O and SO_2 contents in the off-gas and negative correlations for the temperature and the concentration of NO_X and dust in the off-gas. Recirculating flue gas after only removing PM would increase H_2O and SO_2 concentrations, but these species could be reduced through additional gas treatment and could be potential control parameters for adjusting the silica fume quality. As for the negative correlations between SSA and dust concentration, NO_X, and temperature of the off-gas, these are closely related to the silicon yield for the process. For tapping cycles with low yields, a higher amount of SiO was available for combustion, giving higher temperatures and dust concentrations as well as providing the heat needed for thermal NO_X generation. While increased FGR could decrease NO_X formation in the furnace hood, FGR would have no impact on the silicon yield of the process. Discerning the effect of the combustion temperature and the SiO concentration during combustion is challenging since they are connected. Reducing the holding temperature in the small-scale experiment from 1700 to 1650 °C increased the SSA from 22.3 to an average of 32.3 m^2/g, which could be caused by the decreased temperature or by the decreased partial pressure of SiO over the SiO material. Regardless, temperature and/or SiO concentration seem to be more important for the silica fume morphology than whether it is oxidized by O_2 or CO_2.

Condensation products found in CO experiments could point to a mechanism for Si and perhaps SiC contamination in silica fume. During charge burden collapses in the SAF, large amounts of volatiles will be exposed to heat and react at the same time as large amounts of process gas is released. In these situations, periods of oxygen deficiency for combustion could occur over a

https://doi.org/10.1021/acs.iecr.2c03987
Ind. Eng. Chem. Res. 2023, 62, 4246−4259

sufficiently long period for the process gas to cool enough for condensation products to form. Replacing O_2 with CO_2 through FGR might not affect SiO oxidization but might slow down combustion of other volatiles which could contaminate the silica fume. This requires further research.

CONCLUSIONS

CO_2 content in combustion gas does not seem to alter the specific surface of silica fume in controlled small-scale experiments as CO_2 seems to be a sufficient oxidizer of SiO to produce the same particle sizes as seen using synthetic air. However, using different holding temperatures, giving a higher SiO partial pressure, gave a significant increase in the SSA of the PM formed. No signs of alternative condensation reactions were seen with increasing CO_2 concentration. Only when replacing CO_2 with CO were reactions to condensation products favored over amorphous silica spheres.

No significant correlation was found between the FGR rate and the SSA of silica fume formed in the pilot-scale experiments. Although not statistically significant, the correlation was still positive and excluding the tapping cycles without FGR turned this correlation statistically significant. Significant positive correlations were found between silica fume SSA and the concentration of H_2O and SO_2 in the off-gas, which could be potential factors to control silica fume formation industrially through FGR. Significant negative correlations were found between the SSA and the off-gas temperature and the concentration of dust and NO_X in the off-gas. While the moisture content could be controlled through FGR or raw material selection, FGR would have no impact on the silicon yield and dust concentration, which is assumed to be the cause of higher temperatures and NO_X generation. Replacing O_2 with CO_2 in the combustion air might slow down the combustion of volatiles and lead to contamination of the silica fume. The results from the pilot-scale experiment did not answer at which point this becomes a problem and should be investigated further.

ASSOCIATED CONTENT

Supporting Information

The Supporting Information is available free of charge at https://pubs.acs.org/doi/10.1021/acs.iecr.2c03987.

Overview of average values for operational parameters and gas analysis during the periods of silica fume sampling in the pilot-scale experiment (PDF)

AUTHOR INFORMATION

Corresponding Author

Vegar Andersen − *Department of Materials Science and Engineering, NTNU, NO-7491 Trondheim, Norway;* orcid.org/0000-0002-6486-0785; Email: vegar.andersen@ntnu.no

Authors

Kristian Etienne Einarsrud − *Department of Materials Science and Engineering, NTNU, NO-7491 Trondheim, Norway*

Azam Rasouli − *Department of Materials Science and Engineering, NTNU, NO-7491 Trondheim, Norway*

Gabriella Tranell − *Department of Materials Science and Engineering, NTNU, NO-7491 Trondheim, Norway*

Complete contact information is available at: https://pubs.acs.org/10.1021/acs.iecr.2c03987

Notes

The authors declare no competing financial interest.

ACKNOWLEDGMENTS

This work was funded by HighEFF—Centre for an Energy Efficient and Competitive Industry for the Future, an 8 year Research Centre under the FME scheme (Centre for Environment-friendly Energy Research, 257632). The authors gratefully acknowledge the financial support from the Research Council of Norway and user partners of HighEFF.

REFERENCES

(1) Schei, A.; Tuset, J. K.; Tveit, H. *Production of High Silicon Alloys*; TAPIRTrondheim, 1998.

(2) Myhre, B. *Microsilica in Refractory Castables—How Does Microsilica Quality Influence Performance?*: Orlando, Florida, USA, 2005; pp 191−195.

(3) American Concrete Institute. In *Guide for the Use of Silica Fume in Concrete: 234R-06*; Fidjestol, P., Ed.; American Concrete Institute: Farmington Hills, Mich, 2006.

(4) Gür, T. M. Carbon Dioxide Emissions, Capture, Storage and Utilization: Review of Materials, Processes and Technologies. *Prog. Energy Combust. Sci.* **2022**, *89*, 100965.

(5) Arnesen, A. G.; Bjørdal, J. Split Body Closed FeSi75 Furnace. *38th Electric Furnace Conference Proceedings*, 1981; Vol. *38*, pp 191−196.

(6) Dosaj, V. D.; Brumels, M. D.; Haines, C. M.; May, J. B. *Silicon Smelting in a Closed Furnace*; Dow Corning Corporation: Midland: Michigan, 1992.

(7) Dosaj, V. D. *Collection and Conversion of Silicon Furnace Waste Gas into Higher Value Products*; Dow Corning Corporation: Midland: Michigan, 1995.

(8) Mathisen, A.; Normann, F.; Biermann, M.; Skagestad, R.; Haug, A. T. CO2 Capture Oppurtunities in the Norwegian Silicon Industry. *TCCS-10*; Trondheim: Norway, 2019.

(9) Andersen, V.; Knuutila, H. K.; Braakhuis, L.; Myrhaug, E.; Einarsrud, K. E.; Tranell, G. Co2 Capture for the Silicon Process-Effects of Flue Gas Recirculation. In *Proceedings of the 16th International Ferro-Alloys Congress*; Trondheim: Norway, 2021.

(10) Andersen, V.; Solheim, I.; Gaertner, H.; Sægrov-Sorte, B.; Einarsrud, K. E.; Tranell, G. Pilot-Scale Test of Flue Gas Recirculation for The Silicon Process. *J. Sustain. Metall.* **2022**, DOI: 10.1007/s40831-022-00639-0.

(11) Flörke, O. W.; Graetsch, H. A.; Brunk, F.; Benda, L.; Paschen, S.; Bergna, H. E.; Roberts, W. O.; Welsh, W. A.; Libanati, C.; Ettlinger, M.; Kerner, D.; Maier, M.; Meon, W.; Schmoll, R.; Gies, H.; Schiffmann, D. Silica. In *Ullmann's Encyclopedia of Industrial Chemistry*; John Wiley & Sons, Ltd, 2008.

(12) Ulrich, G. D. Theory of Particle Formation and Growth in Oxide Synthesis Flames. *Combust. Sci. Technol.* **1971**, *4*, 47−57.

(13) Ulrich, G. D.; Milnes, B. A.; Subramanian, N. S. Particle Growth in Flames. II: Experimental Results for Silica Particles. *Combust. Sci. Technol.* **1976**, *14*, 243−249.

(14) Ulrich, G. D.; Subramanian, N. S. III. Coalescence as a Rate-Controlling Process. *Combust. Sci. Technol.* **1977**, *17*, 119−126.

(15) Pratsinis, S. E.; Vemury, S. Particle Formation in Gases: A Review. *Powder Technol.* **1996**, *88*, 267−273.

(16) Pratsinis, S. E. Flame Aerosol Synthesis of Ceramic Powders. *Prog. Energy Combust. Sci.* **1998**, *24*, 197−219.

(17) Buesser, B.; Pratsinis, S. E. Design of Nanomaterial Synthesis by Aerosol Processes. *Annu. Rev. Chem. Biomol. Eng.* **2012**, *3*, 103−127.

(18) Friedlander, S. K. Smoke, Dust, and Haze: Fundamentals of Aerosol Dynamics, 2nd ed.; *Topics in Chemical Engineering*; Oxford University Press: New York, 2000.

(19) González-Fariña, R. Modelling the Mechanisms of Microsilica Particle Formation and Growth. Ph.D. Thesis, University of Oxford, 2020. https://ora.ox.ac.uk/objects/uuid:df016039-4c40-43ca-91a6-ffe0575aae77 (accessed April 10, 2022).

(20) Kamfjord, N. E. Mass and Energy Balances of the Silicon Process. Ph.D. Thesis, NTNU, Trondheim, Norway, 2012.
(21) Roine, A. HSC Chemistry, 2020. https://www.hsc-chemistry.com/ (accessed 11 23, 2022).
(22) Andrea, A.; Merete, M. Condensation of SiO and CO in Silicon Production-A Literature Review. In *Extraction 2018; The Minerals, Metals & Materials Series*; Springer International Publishing: Cham, 2018; pp 697−716.
(23) Broggi, A.; Tangstad, M.; Ringdalen, E. Characterization of a Si-SiO2 Mixture Generated from SiO(g) and CO(g). *Metall. Mater. Trans. B* **2019**, *50*, 2667−2680.
(24) Broggi, A.; Ringdalen, E.; Tangstad, M. Characterization, Thermodynamics and Mechanism of Formation of SiC-SiOx Core-Shell Nanowires. *Metall. Mater. Trans. B* **2021**, *52*, 339−350.
(25) Andersen, V.; Solheim, I.; Gaertner, H.; Sægrov-Sorte, B.; Einarsrud, K. E.; Tranell, G. Pilot Scale Test of Flue Gas Recirculation for the Silicon Process. In *REWAS 2022: Developing Tomorrow's Technical Cycles (Volume I); The Minerals, Metals & Materials Series*; Springer International Publishing: Anaheim: California, USA, 2022; pp 555−564. DOI: DOI: 10.1007/978-3-030-92563-5_58.
(26) Cyr, M.; Tagnit-Hamou, A. Particle Size Distribution of Fine Powders by LASER Diffraction Spectrometry. Case of Cementitious Materials. *Mat. Struct.* **2001**, *34*, 342−350.
(27) 844 Series Combustion Analyzer. LECO Corporation. https://www.leco.com/product/844-series (accessed Dec 16, 2022).
(28) 836 Series Elemental Analyzer. LECO Corporation. https://www.leco.com/product/836-series (accessed Dec 16, 2022).
(29) Madsen, I. C.; Scarlett, N. V. Y.; Kern, A. Description and Survey of Methodologies for the Determination of Amorphous Content via X-Ray Powder Diffraction. *Prog. Energy Combust. Sci.* **2011**, *226*, 944−955.
(30) Friede, B. Microsilica—Characterization of an Unique Additive. *Proceedings of the 10th International Inorganic-Bonded Fiber Composites Conference (IIBCC 2006)—Sao Paulo, Brazil, Universidade de Sao Paulo and University of Idaho*; Universidade de Sao Paulo & University of Idaho: Sao Paulo: Brazil, 2006.
(31) Ksiazek, M.; Kero, I.; Wittgens, B. Challenges in Transporting the Off-Gasses from the Silicon Process. *Takano International Symposium on Metals and Alloys*, 2015; Vol. 3, p 10..
(32) Vangskåsen, J.; Høgsand, Ø. *Investigation of Cavity and Condensate Formation in the Silicon Process*. Intern; NTNU: Trondheim, Norway 2011.
(33) Aarnæs, T. S.; Tangstad, M.; Ringdalen, E. SiC Formation and SiO Reactivity of Methane at High Temperatures. *Mater. Chem. Phys.* **2022**, *276*, 125355.
(34) Kamfjord, N. E.; Tveit, H.; Naess, M. K.; Myrhaug, E. H. Mechanisms of NO Formation during SiO Combustion. In *3rd International Symposium on High-Temperature Metallurgical Processing*; John Wiley & Sons, Ltd, 2012; pp 401−409. DOI: DOI: 10.1002/9781118364987.ch49.

https://doi.org/10.1021/acs.iecr.2c03987
Ind. Eng. Chem. Res. 2023, 62, 4246−4259